Theoretical Investigation into Competing Unimolecular Reactions Encountered in the Pyrolysis of Acetamide

ARTICLE *in* THE JOURNAL OF PHYSICAL CHEMISTRY A · DECEMBER 2011

Impact Factor: 2.69 · DOI: 10.1021/jp2067765 · Source: PubMed

THE JOURNAL OF PHYSICAL CHEMISTRY A

ARTICLE

pubs.acs.org/JPCA

Theoretical Investigation into Competing Unimolecular Reactions Encountered in the Pyrolysis of Acetamide

Mohammednoor Altarawneh,*[,†] Ala'a H. Al-Muhtaseb,[‡] Mansour H. Almatarneh,[§] Raymond A. Poirier,[⊥] Niveen W. Assaf,[†] and Khalid K. Altarawneh[∥]

[†]Department of Chemical Engineering, Al-Hussein Bin Talal University, Ma'an, Jordan

[‡]Petrolume and Chemical Engineering Department, Faculty of Engineering, Sultan Qaboos University, Sultanate of Oman

[§]Department of Chemistry, Memorial University-Grenfell Campus, Corner Brook, Newfoundland A2H 6P9, Canada

[⊥]Department of Chemistry, Memorial University, St. John's, Newfoundland A1B 3X7, Canada

[∥]Faculty of Engineering, Philadelphia University, Amman, Jordan

Supporting Information

ABSTRACT: Motivated by the necessity to understand the pyrolysis of alkylated amines, unimolecular decomposition of acetamide is investigated herein as a model compound. Standard heats of formation, entropies, and heat capacities, are calculated for all products and transition structures using several accurate theoretical levels. The potential energy surface is mapped out for all possible channels encountered in the pyrolysis of acetamide. The formation of acetamedic acid and 1-aminoethenol and their subsequent decomposition pathways are found to afford the two most energetically favored pathways. However, RRKM analysis shows that the fate of acetamedic acid and 1-aminoethenol at all temperatures and pressures is to reisomerize to the parent acetamide. 1-Aminoethenol, in particular, is predicted to be a long-lived species enabling its participation in bimolecular reactions that lead to the formation of the major experimental products. Results presented herein reflect the importance of bimolecular reactions involving acetamide and 1-aminoethenol in building a robust model for the pyrolysis of N-alkylated amides.

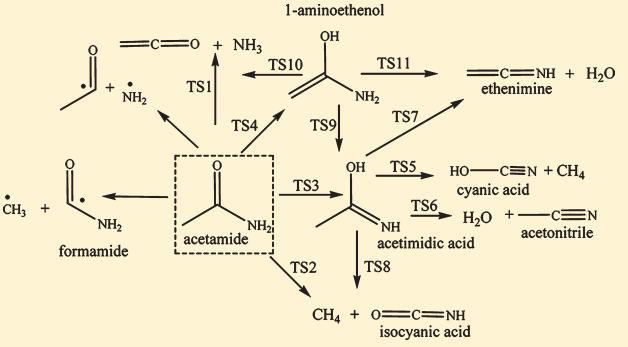

1. INTRODUCTION

Most interest in studying the acetamide (CH_3CONH_2) molecule stems from its importance as a model of peptide bonds in biological molecules,[1] in addition to its carcinogenic effects.[2,3] Acetamide constitutes a dominant N-containing product from the fragmentation of soil organic matter,[4] biomass,[5,6] sewage sludge,[7] and explosives.[8] It is believed that the major source of acetamide comes from the rupture of the amino polysaccharide linkages present in chitin, that is, the second largest structural block in biomass.[9,10] Acetamide is also produced in appreciable concentrations from the pyrolysis of peptides,[11] fungi,[9] bacteria cells,[12] and humic and fluvic acids.[3]

A great deal of research has focused on revealing the mechanism of the hydrolysis of acetamide.[13−15] Hydrolysis of acetamide is widely accepted to be dominated by a nucleophilic attack by a water molecule on the carbonyl oxygen and the formation of O-protonated tautometer.[14] However, little is known regarding the mechanism for the homogeneous gas phase pyrolysis. Generally, the pyrolysis of N-alkylated amides is thought to proceed in a way analogous to the pyrolysis of esters.[16] The presence of other distinct decomposition routes is also possible because of the presence of the amine group.[17] The consensus in the literature is that the major decomposition products are ammonia (NH_3), acetic acid (CH_3COOH), and methyl cyanide or acetonitrile (CH_3CN).[4,17] Observation of water and methane as secondary products was attributed to the competing decarboxylation and dehydration channels in the unimolecular decomposition of acetic acid;[18]

$$CH_3COOH \rightarrow CH_4 + CO_2$$
$$CH_3COOH \rightarrow CH_2CO + H_2O$$

Aspden et al.[17] found that the self-reaction of acetamide affording ammonia, acetic acid, and acetonitrile accounts satisfactorily for atomic stoichiometry for up to 60% of the pyrolysis progress. For the remaining products, bimolecular reactions involving acetamide, water, and acetic acid become important. On the other hand, photodissociation of acetamide is found to

Received: July 15, 2011
Revised: October 22, 2011
Published: October 25, 2011

Table 1. Reaction Energies (ΔE) and Activation Energies ($\Delta E^{\ddagger}$) for Reactions in the Unimolecular Decomposition of Acetamide

		$\Delta E^{\ddagger}$					ΔE				
reaction	TS	BB1K	MP2	G3B3	G3MP2B3	CBS-QB3	BB1K	MP2	G3B3	G3MP2B3	CBS-QB3[e]
$CH_3CONH_2 \rightarrow CONH_2 + CH_3$							86.7	86.3	86.9	85.6	87.0
$CH_3CONH_2 \rightarrow O{=}C{-}CH_3 + NH_2$							98.4	98.7	97.6	95.3	97.6
$CH_3CONH_2 \rightarrow O{=}C{=}CH_2 + NH_3$	TS1	73.4	71.2	73.7	73.8	74.3	34.6	33.5	33.7	31.5	33.1
$CH_3CONH_2 \rightarrow O{=}C{=}NH + CH_4$	TS2	80.7	77.5	80.7	80.5	81.0	11.0	7.6	9.3	8.0	8.6
$CH_3CONH_2 \rightarrow CH_3C(OH)NH$	TS3	43.1	42.1	42.6	42.6	42.8	12.2	11.3	11.0	10.9	11.5
$CH_3CONH_2 \rightarrow CH_2C(OH)NH_2$	TS4	62.8	64.1	64.2	64.4	64.9	24.1	25.5	24.1	23.7	24.5
$CH_3C(OH)NH \rightarrow N{\equiv}C{-}OH + CH_4$	TS5	104.5	100.0	103.0	102.13	102.1	24.4	18.9	23.1	21.7	22.0
$CH_3C(OH)NH \rightarrow N{\equiv}C{-}CH_3 + H_2O$	TS6	64.3	58.1	60.6	60.3	60.9	7.9	−1.4	3.1	3.0	4.0
$CH_3C(OH)NH \rightarrow HN{=}C{=}CH_2 + H_2O$	TS7	80.6	79.4	81.2	81.0	81.6	42.7	43.6	42.5	43.1	44.0
$CH_3C(OH)NH \rightarrow HN{=}C{=}CH_2 + H_2O$	TS8	79.6	78.4	80.2	80.0	79.9	−1.2	−3.6	−1.7	−2.9	−2.9
$CH_3C(OH)NH \rightarrow HN{=}C{=}CH_2 + H_2O$	TS9	54.2	53.3	54.8	54.6	54.7	11.5	14.0	13.6	12.8	13.0
$CH_3C(OH)NH \rightarrow HN{=}C{=}CH_2 + H_2O$	TS10	38.8	36.7	39.0	38.0	38.2	9.1	6.3	8.1	7.8	8.7
$CH_3C(OH)NH \rightarrow HN{=}C{=}CH_2 + H_2O$	TS11	61.4	59.1	61.6	60.7	60.8	31.3	29.6	30.8	30.3	31.0

afford four channels: namely, $CH_3 + CONH_2$, $CH_3CO + NH_2$, $CH_3CN + H_2O$, and $CH_3NH_2 + CO$.[19] Hydrolysis of acetamide in supercritical water (SCW) is also found to produce ammonia and acetic acid as the major products,[20] in which the decay of acetamide was described as a first-order reaction with respect to the concentration of acetamide.

In this study, a detailed theoretical investigation of the homogeneous gas-phase pyrolysis of acetamide is carried out to provide a mechanism that is consistent with the available experimental findings. Our primary aim is to account qualitatively for the contribution of unimolecularly derived routes in the overall mechanism for the pyrolysis of acetamide. It is hoped that this study will provide kinetic input for the construction of reaction models that account satisfactorily for the decomposition of acetamide as a model compound of alkylated amides; that is, dominant N-containing species from the pyrolysis of various types of fuels.

2. COMPUTATIONAL METHODS

The Gaussian03[21] suite of programs was used to carry out all structure/geometry optimizations. The potential energy surface (PES) for the unimolecular decomposition of acetamide was investigated using various theoretical methods. Composite methods of G3B3,[22a,b] G3MP2B3,[23,22b] and CBS-QB3[24a,b] are used to calculate reaction and activation energies. These methods are based on performing successive single-point energy calculations using accurate theoretical approaches on preoptimized structures. Both G3B3 and G3MP2B3 methods are utilized to obtain accurate energies for structures optimized at the B3LYP[25]/6-31G(d) level of theory. G3MP2B3 energies are based on energies optimized at the B3LYP/6-31G(d) level of theory. CBS-QB3 is a five-step method that starts with B3LYP/CBSB7 geometry and frequency calculations, followed by CCSD(T), MP4SDQ, and MP2 single-point calculations and then a CBS extrapolation and a term for spin contamination.[24]

The BB1K[26] hybrid meta-GGA density functional was shown to outperform other density functional theory methods in estimating reaction barriers and geometries of transition state structures when compared with wave function theories, especially MPn theory.[27] In addition to using a Hartree−Fock (HF) exchange fraction of 0.42 (compared with 0.20 for other functionals, such as B3LYP), the BB1K method also derives kinetic energy density from Kohn−Sham orbitals by using the kinetic-energy-dependent dynamical correlation functional BB95. In this study, reaction and activation energies for all unimolecular reactions are calculated at the BB1K/GTlarge[28] and MP2[29]/6-311+G(d,p) levels of theory to assess the relative performance of BB1K and MP2.

Rate constants for the high-pressure limit are calculated within the formalism of transition state theory (TST)[30] for all reactions in the unimolecular decomposition of acetamide. In these calculations, degrees of freedom corresponding to internal rotations are treated as hindered rotors. The necessity and the methodology of applying this treatment is well described in the literature.[31] All rate constant calculations are carried out using the Chemrate code.[32] The effect of quantum tunneling on the rate constants was modeled using a one-dimensional Eckart formalism[33] as implemented in the Chemrate code. The rate constant for one barrierless reaction is obtained by the variation transition state theory (VTST). The implementation of the VTST is thoroughly detailed in many recent studies.[34−36] In the VTST formalism, the reaction rate constant is minimized as a function of reaction coordinate (s) and temperature (T):

$$\overset{\mathrm{VTST}}{k}(T) = \min \overset{\mathrm{TST}}{k}(s, T)$$

where $\overset{\mathrm{TST}}{k}$ signifies the reaction rate constant from the TST. Pressure-dependent reaction rate constants are obtained from RRKM theory.[37] The bath gas is helium, and the collisional energy transfer is described using an exponential-down model with $\Delta E_{\mathrm{down}} = 200\ \mathrm{cm}^{-1}$. The choice of this value follows the recommendation by Carstensen and Dean[38] to simulate the

dx.doi.org/10.1021/jp2067765 |J. Phys. Chem. A 2011, 115, 14092–14099

behavior of He as a weak collider. Lennard-Jones parameters used for the acetamide are σ = 4.705 Å and κ/ε_b = 383.05 K.[39]

3. RESULTS AND DISCUSSIONS

3.1. Unimolecular Decomposition of Acetamide. *3.1.1. Potential Energy Surface (PES) for the Unimolecular Decomposition of Acetamide.* Various theoretical studies on acetamide focused on finding its equilibrium structure in terms of its planarity.[40−42] The consensus in the literature is that there is a slight deviation from C_s symmetry due to the methyl group. Our optimized C_1 acetamide structure at the B3LYP/6-31G(d) predicts that the methyl group deviates by 0.67° from planarity. The NH_2 group resides in a plane with the rest of the molecule, in accord with the experimental measurements.[43,44] BB1K and MP2 methods also yield a near-planar structure.

Reaction and activation energies for individual reactions are given in Table 1 for the five theoretical methods. Activation energies ($\Delta E^{\ddagger}$) calculated by the three composite methods, G3B3, G3MP2B3, and CBS-QB3, are found to be in very good agreement, that is, within 1.0 kcal/mol. Generally, $\Delta E^{\ddagger}$ values calculated by the BB1K method are very close to the corresponding average values of the three composite methods, in which the absolute average difference is calculated to be 1.0 kcal/mol. The corresponding absolute average difference of the MP2 method is found to amount to 1.8 kcal/mol. This finding is consistent with the reported performance of the BB1K functional in predicting activation energies. The BB1K and MP2 activation energies are all within 4.5 kcal/mol from the average $\Delta E^{\ddagger}$ values of the three composite methods. Reaction energies (ΔE) obtained by the three composite methods are also in excellent agreement, with absolute differences within 2.3 kcal/mol. In general, the five deployed theoretical methods are found to produce comparable energetics, for which the three composite methods, in particular, provide very accurate representation of the PES.

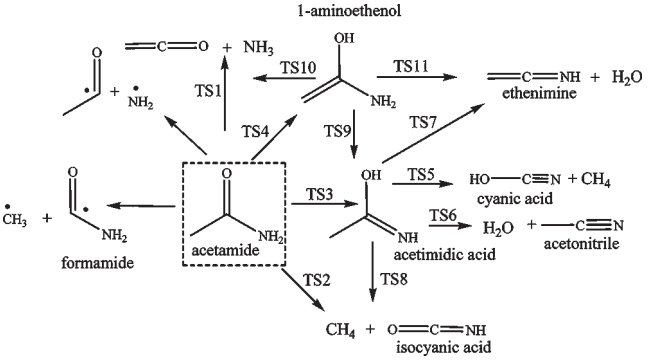

Figure 1. Mechanism and structures of the unimolecular decomposition of acetamide.

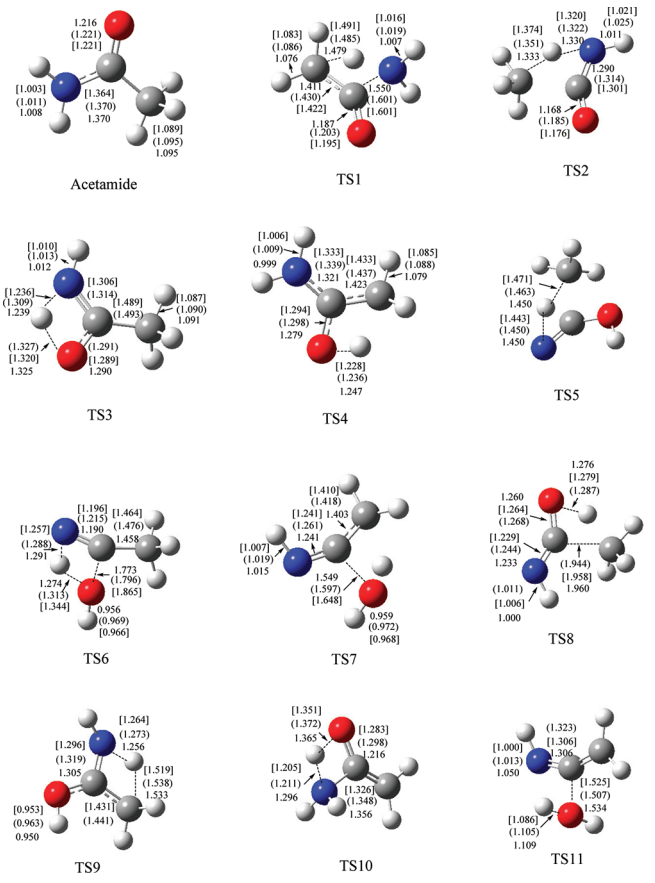

Figure 3. Geometries of acetamide and transition structures for the unimolecular decomposition of aacetamide. Values in parentheses are calculated at the BB1K/GTlarge; in brackets, at the MP2/6-311+G(d,p) level; and other values, at the B3LYP/6-31G(d) level of theory.

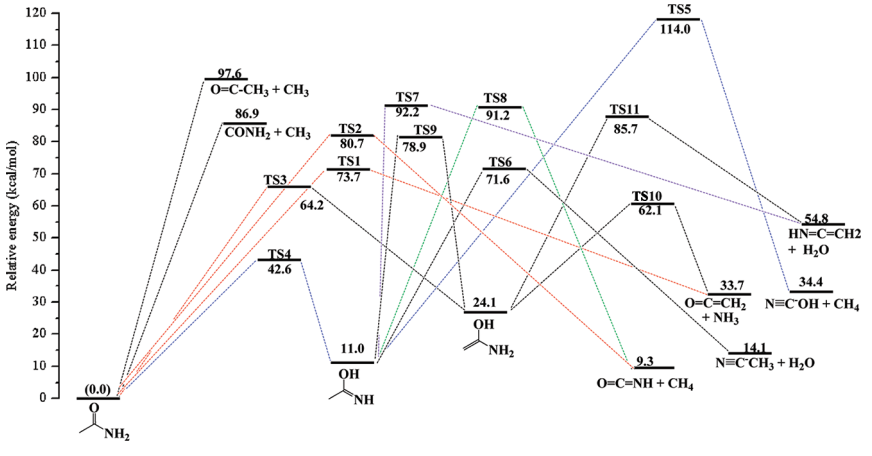

Figure 2. PES for the unimolecular decomposition of acetamide mapped out at the G3B3 theory.

dx.doi.org/10.1021/jp2067765 |J. Phys. Chem. A 2011, 115, 14092–14099

All plausible pathways in the unimolecular decomposition of acetamide on the singlet ground state are depicted in Figure 1. The PES is mapped out in Figure 2. Optimized geometries for transition state structures are shown in Figure 3, along with the optimized structure of acetamide. Overall, there are six distinct initial pathways. Acetamide fragmentation into $CONH_2 + CH_3$ and $O{=}C{=}CH_3 + NH_2$ are found to occur without encountering a first-order saddle point (quantum chemical TS) on the PES. The C−C and C−N bond dissociations are predicted to be endoergic by 85.6−86.9 and 95.3−98.7 kcal/mol, respectively. Thus, the calculated C−C bond energy in $H_3C{-}CONH_2$ is substantially lower than the well-established corresponding C−C bond in acetic acid, that is, 92.0 kcal/mol.[45]

Direct expulsion of ammonia from acetamide takes place via transition state structure TS1. TS1 involves a migration of one of the methyl hydrogen to the neighboring NH_2 group and the subsequent departure of a molecule of ammonia. This is evident from the geometry of TS1 shown in Figure 3, where the three methods show similar geometrical features; namely, within 0.01 Å. The calculated activation energies range from 71.2 to 73.8 kcal/mol, and the separated products ($O{=}C{=}CH_2$ (ethenone) + NH_3) reside 31.5−34.6 kcal/mol above the entrance channel. Unimolecular decomposition of acetamide can afford methane (CH_4) via transition state structure TS2, which involves the transfer of one of the H atoms in the amine group to the methyl group, followed by the expulsion of methane and isocyanic acid ($O{=}C{=}NH$). TS2 is predicted to be 77.5 kcal/mol (at MP2) to 80.7 kcal/mol (at BB1K) higher than the acetamide molecule. The formation of methane and isocyanic acid ($O{=}C{=}NH$) through this channel is associated with a modest endoergicity in the range of 7.6−11.0 kcal/mol.

As shown in Figure 1, two enolization processes can take place in the unimolecular decomposition of acetamide. 1-Aminoethenol ($CH_2C(OH)NH_2$) can form from the migration of one of the H atoms in the methyl group to the ketonic oxygen via TS4 with an activation energy of 62.8−64.4 kcal/mol above the entrance channel. Formation of 1-aminoethenol is predicted to be endoergic by 23.7−25.5 kcal/mol. The analogous process in acetic acid, leading to the formation of enediol (1,1-ethenediol) via a 1,3-hydrogen migration shift from the methyl group, was found to require 73.1 kcal/mol of activation energy.[46] The difference in the activation energies for this enolization process between acetamide and acetic acid is in accord with the calculated difference in C−C bond energies in these two molecules.[45]

Enolization via the transfer of a hydrogen atom from the amine group to the ketonic oxygen via TS3 is found to be more favorable both thermodynamically and kinetically. Formation of acetimidic acid ($CH_3C(OH)NH$) occurs via the four-center transition structure TS3 with an activation barrier in the range of 42.1−43.1 kcal/mol with a 10.9−12.2 kcal/mol endoergicity.

Since acetimidic acid is the most plausible product from the initial unimolecular rearrangement of acetamide, possible exit channels for acetimidic acid are further characterized. Decomposition of acetimidic acid affords four pathways, as evident from Figures 1 and 2. The dehydration of acetimidic acid into water and acetonitrile ($N{\equiv}C{-}CH_3$) occurs through the four-centered transition state structure TS6 in which the transfer of a hydrogen atom from the NH group is accompanied by the rupture of the C−OH bond and the formation of a water molecule. This dehydration channel is associated with an activation barrier of 58.1 kcal/mol at (MP2) to 64.3 kcal/mol (at BB1K). MP2 predicts that this channel is thermodynamically neutral, whereas

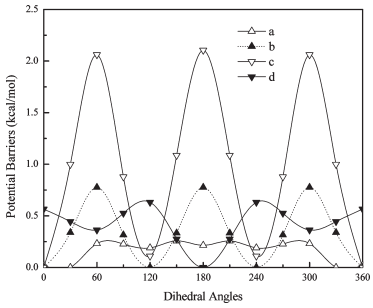

Figure 4. Internal rotors' potentials for the rotation of the methyl group in acetamide (a), acetimidic acid (b), and TS3 (d) and the torsion around the OH bond in acetimidic acid (c) at the B3LYP/6-31G(d,p) level.

the BB1K yields a modest endoergicity of 9.7 kcal/mol. The other dehydration channel is characterized by the formation of ethenimine and water. This process takes place via the four-centered transition state structure TS7, in which the hydroxyl group and a hydrogen atom from the methyl group depart from the molecule in a concerted movement, forming a water molecule. This process encounters a sizable activation barrier (79.4−81.2 kcal/mol) and substantial reaction energy (42.7−43.6 kcal/mol).

As depicted in the reaction scheme in Figure 1, methane can be formed from acetimidic acid through two channels: via TS5 and TS8. Formation of cyanic acid ($N{\equiv}C{-}OH$) and methane proceed via the transfer of a hydrogen atom from the NH group and the concerted departure of a methane molecule as characterized by TS5. The lowest barrier calculated for this process is predicted to be 100.0 kcal/mol at the MP2 level, and the highest barrier is estimated to be 104.5 kcal/mol at the BB1K level. The second pathway involves the formation of methane alongside isocyanic acid through TS8 that is located 78.4−80.2 kcal/mol above the entrance channel of acetimidic acid. This process is predicted to be associated with an exoergicity of only −1.2 to −3.6 kcal/mol.

The fate of 1-aminoethenol is also illustrated in Figures 1 and 2. 1-Aminoethenol can produce acetimidic acid via TS9 through an activation barrier in the range of 53.3−54.8 kcal/mol. Formation of ammonia from 1-aminoethenol (TS10) represents its most plausible exit channel and requires 22.4−22.7 kcal/mol less activation energy than that needed for the formation of water (TS11).

By inspecting the PES of Figure 2, two pathways can be marked as the most favorable energetically: (1) acetamide → TS4 → 1-aminoethenol → TS10 → $NH_3 + O{=}C{=}CH_2$, with an overall activation barrier of 64.3 kcal/mol; and (2) acetamide → TS3 → acetimidic acid → TS6 → $H_2O + N{\equiv}C{-}CH_3$, with an overall activation barrier of 71.6 kcal/mol. This observation agrees qualitatively with the fact that ammonia and acetonitrile are among the three most important experimental products from the pyrolysis of acetamide.

3.2. Entropies and Heat Capacities. Accurate estimations of reaction rate constants based on transition state theory requires treating the internal rotation modes in reactants and transition structures as hindered rotors rather than harmonic oscillators. The procedure and necessity for this treatment is described elsewhere.[31] Profiles for these rotations are obtained by performing partial optimization in molecules and energy scanning in transition structures at an interval of 30° at the B3LYP/6-31+G(d,p)

Table 2. $S_{298}°$ in cal/(mol K) and $C_p°(T)$ in cal/(mol K)

		$C_p°(T)$				
	$S_{298}°$	298.15 K	500 K	800 K	1000 K	1500 K
CH_3CONH_2	74.99	18.90	26.26	33.56	36.86	42.07
$CH_3C(OH)NH$	70.91	17.78	25.87	33.51	36.86	42.09
TS1	69.76	17.95	25.83	33.07	36.19	40.98
TS2	71.18	17.12	24.71	32.41	35.79	40.85
TS3	69.21	17.89	25.77	32.99	36.11	40.88
TS4	71.80	19.29	26.58	33.54	36.63	41.32
TS5	70.26	19.08	27.02	33.78	36.67	41.16
TS6	72.86	19.52	26.51	33.35	36.41	41.11
TS7	74.10	20.77	27.44	33.76	36.65	41.19
TS8	71.96	19.76	27.10	33.84	36.81	41.36
TS9	68.35	17.15	25.40	32.72	35.85	40.67
TS10	68.74	16.93	24.82	32.22	35.44	40.45
TS11	69.55	18.52	26.27	33.00	35.94	40.61
$CH_2C(OH)NH_2$	71.01	19.63	27.40	34.16	37.15	42.03
$O=C=CH_2$	61.50	12.45	15.77	18.87	20.31	22.59
$N\equiv C-CH_3$	62.59	12.57	16.77	21.42	23.63	27.08
$CONH_2$	62.90	12.54	15.66	18.72	20.11	22.36
CH_3	50.99	9.41	10.96	12.99	14.18	16.35
$O=C=NH$	59.36	10.97	13.31	15.32	16.22	17.67
$N\equiv C-OH$	60.07	11.11	13.27	15.25	16.15	17.61
$HN=C=CH_2$	70.67	16.01	19.58	22.88	24.50	27.29

level of theory. For instance, Figure 4 depicts the energy profiles for methyl group rotation in acetamide (a), acetimidic acid (b), and TS3 (c) and the rotation around the O−H bond in acetimidic acid (d). Barriers for methyl group rotation are 0.26, 0.63, and 0.77 kcal/mol in acetamide, acetimidic acid, and TS3, respectively. The calculated entropies of formation at 298 K ($S_{298}°$) and heat capacities ($C_p°(T)$) at specified temperatures based on optimized structures, rotational constants, and vibrational frequencies obtained using the B3LYP/GTlarge method are given in Table 2.

3.3. Reaction Rate Parameters. Reaction rate constants at the high-pressure limit, $k(T, \text{high-}P)$ are calculated for the plausible channels in the unimolecular decomposition of acetamide. Rate constants are fitted for a temperature range of 300−2000 K to modified Arrhenius parameters, $k(T, \text{high}-P) = AT^n \exp(-E_a/RT)$, where A is the pre-exponential factor, n is a unitless parameter, and E_a is the energy of activation. Rate constant parameters are given in Table 3. Arrhenius parameters are also obtained for the high-pressure limit rate constant of the possible unimolecular decomposition of acetimidic acid and 1-aminoethenol.

Since the C−N direct bond fission requires an additional energy of 10.0 kcal/mol in comparison with the C−C bond fission, the reaction rate constant is calculated only for the fragmentation reaction $CH_3CONH_2 \rightarrow CONH_2 + CH_3$. The reaction rate constant for this particular reaction is calculated on the basis of the variational transition state theory. Partial optimization is carried out at an interval of 0.100 Å along the reaction coordinate, that is, $H_3C\cdots CONH_2$ elongation, at the G3MP2B3 level of theory. The minimum energy point (MEP) profile for $H_3C\cdots CONH_2$ elongation is depicted in Figure 5. VTST requires the minimization of the reaction rate coefficient along the reaction coordinate, that is, spacing between CH_3 and $CONH_2$, for each temperature. The decomposition reaction is found to be controlled with a loose 3.100 Å transition structure throughout the temperature interval of 300−2000 K. The resulting A-factor term ($2.00 \times 10^{12}\ T^{0.91}\ s^{-1}$) is in agreement with the literature values for the A-factor of CH_3 expulsion from various molecules.[48] For instance, our A-factor term at 1000 K is $1.1 \times 10^{15}\ s^{-1}$, whereas the A factor for the methyl group expulsion from acetaldehyde is measured to be $6.0 \times 10^{14}\ s^{-1}$ in the temperature interval of 1000−1700 K.[47] Arrhenius parameters for the other four channels are derived using TST on the basis of their corresponding transition state structures. Reaction rate constants at the high-pressure limits are given in Table 3.

To simulate realistic conditions encountered in the pyrolysis environment, reaction rates for all decomposition channels are calculated as a function of temperature and pressure using RRKM theory. As an example of pressure-dependent rate constants, apparent rate parameters at 1 atm are given in Table 4.

Table 3. High-Pressure Limit Arrhenius Rate Parameters for Reactions in the Unimolecular Decomposition of Acetamide

reaction	$A\ (s^{-1})$	n	E_a/R (K)
$CH_3CONH_2 \rightarrow CONH_2 + CH_3$	2.54×10^{12}	0.92	40 100
$CH_3CONH_2 \rightarrow O=C=CH_2 + NH_3$	1.70×10^{10}	0.69	37 200
$CH_3CONH_2 \rightarrow O=C=NH + CH_4$	6.25×10^{9}	0.96	53 100
$CH_3CONH_2 \rightarrow CH_2C(OH)NH_2$	1.84×10^{12}	0.00	32 400
$CH_3CONH_2 \rightarrow CH_3C(OH)NH$	3.23×10^{12}	0.00	21 600
$CH_3C(OH)NH \rightarrow N\equiv C-OH + CH_4$	5.00×10^{10}	1.18	51 900
$CH_3C(OH)NH \rightarrow N\equiv C-CH_3 + H_2O$	1.12×10^{11}	0.95	30 000
$CH_3C(OH)NH \rightarrow HN=C=CH_2 + H_2O$	9.33×10^{9}	1.17	40 900
$CH_3C(OH)NH \rightarrow O=C=NH + CH_4$	1.56×10^{10}	1.15	40 400
$CH_2C(OH)NH_2 \rightarrow CH_3C(OH)NH$	9.12×10^{11}	0.20	27 400
$CH_2C(OH)NH_2 \rightarrow O=C=CH_2 + NH_3$	5.10×10^{11}	0.00	19 800
$CH_2C(OH)NH_2 \rightarrow HN=C=CH_2 + H_2O$	6.30×10^{11}	0.39	31 200

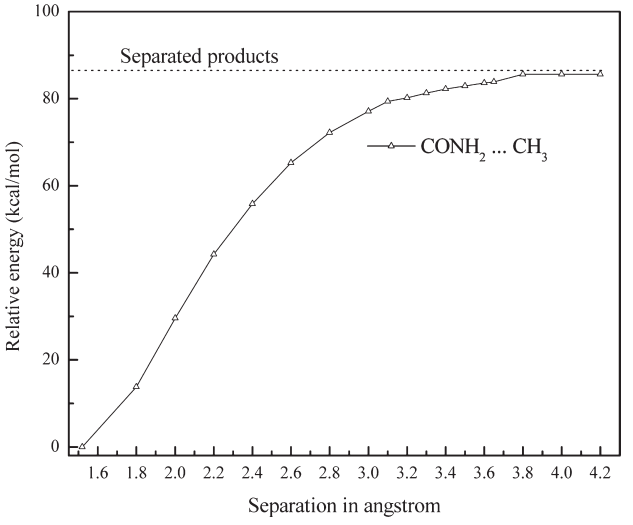

Figure 5. Minimum energy points (MEP) curve for the fragmentation reaction $CH_3CONH_2 \rightarrow CONH_2 + CH_3$ calculated at the G3MP2B3 level of theory.

Table 4. Apparent Rate Parameters ($\grave{A}$, n, E_a) for the Decomposition of Acetamide and Acetamedic Acid at 1 atm

reaction	$\grave{A}$ (s^{-1})	n	E_a/R (K)
$CH_3CONH_2 \rightarrow CONH_2 + CH_3$	3.16×10^{67}	−17.81	46 000
$CH_3CONH_2 \rightarrow O{=}C{=}CH_2 + NH_3$	2.00×10^{62}	−16.52	42 000
$CH_3CONH_2 \rightarrow O{=}C{=}NH + CH_4$	1.26×10^{58}	−14.96	43 700
$CH_3CONH_2 \rightarrow CH_2C(OH)NH_2$	4.10×10^{63}	−16.32	46 000
$CH_3CONH_2 \rightarrow CH_3C(OH)NH$	1.59×10^{88}	−25.53	60 500
$CH_3C(OH)NH \rightarrow CH_3CONH_2$	3.72×10^{19}	−5.62	19 900
$CH_3C(OH)NH \rightarrow CH_2C(OH)NH_2$	6.31×10^{19}	−9.60	39 000
$CH_3C(OH)NH \rightarrow N{\equiv}OH + CH_4$	2.12×10^{87}	−24.63	62 000
$CH_3C(OH)NH \rightarrow N{\equiv}C{-}CH_3 + H_2O$	4.00×10^{33}	−6.12	34 000
$CH_3C(OH)NH \rightarrow HN{=}C{=}CH_2 + H_2O$	5.05×10^{57}	−14.21	56 000
$CH_3C(OH)NH \rightarrow O{=}C{=}NH + CH_4$	6.31×10^{56}	−13.77	48 000

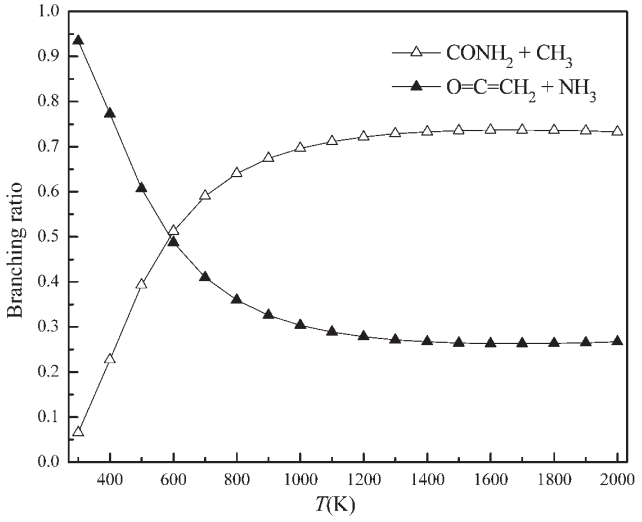

Figure 6. Branching ratio for the $CONH_2 + CH_3$ and $O{=}C{=}CH_2 + NH_3$ channels at 1 atm.

The five initial decomposition channels of acetamide are found to exhibit strong pressure-dependent behavior, especially at high pressures. For instance, the ratios of k_{atm}/k_∞ at 800 K for the three channels leading to $CONH_2 + CH_3$, $CH_2C(OH)NH_2$, and $CH_3C(OH)NH$ are calculated to be 0.007, 0.35 and 0.64, respectively. This indicates that the falloff region extends notably beyond the atmospheric pressures, especially for the $CONH_2 + CH_3$ channel.

According to the expressions for the reaction rate constants in Table 4, initial decay of acetamide is solely dominated by the enolization into acetimidic acid. The contribution from the other channels is predicted to be negligible at all temperatures. For acetic acid,[46] the enolization process associated with a 1,3-hydrogen shift leading to enediol is also found to be the dominant channel at lower and intermediate temperatures. However, kinetic analysis for the six available exit channels of the acetamedic acid reveals that the fate of atmospheric acetamedic acid is solely controlled by the reverse reaction of $CH_3C(OH)NH \rightarrow CH_3CONH_2$ at all temperatures. The lifetime of acetamedic acid at 800 K is calculated to be 7.65×10^{-4} s.

1-Aminoethenol is also found to predominantly reform acetamide at all temperatures, however, with a noticeably longer lifetime of 0.12 s at 800 K. This indicates that acetamedic acid is a too short-lived species to participate in bimolecular reactions, but 1-aminoethenol is expected to be a long-lived species, enabling its bimolecular reactions either with the parent acetamide or its self-condensation. Accordingly, direct decomposition of acetamide is unlikely to contribute to the formation of the major experimental product of acetonitrile.

By the exclusion of the contribution of the two channels into 1-aminoethenol and acetamedic in view of their high reversibility into the parent acetamide, the eventual decay of acetamide is found to proceed through the two channels into $CONH_2 + CH_3$ and $O{=}C{=}CH_2 + NH_3$. Branching ratios at 1 atm for these two channels are plotted in Figure 6. At temperatures below 600 K, fragmentation leading to the formation of $CONH_2$ and CH_3 radicals is predicted to prevail, whereas beyond this temperature, formation of ammonia and ethenone becomes more important. Decarboxylation into $CO_2 + CH_4$ and 1,3-hydrogen shift leading to enediol during the pyrolysis of acetic acid is found to be a competitive channel at elevated temperatures.[48] In comparison, the corresponding process in the pyrolysis of acetamide leading to the formation of methane ($CH_3CONH_2 \rightarrow O{=}C{=}NH + CH_4$) is associated with a very minor contribution.

The results herein suggest that unimolecular decomposition of acetamide cannot explain by itself the overall reaction sequences operating under the pyrolysis of acetamide. Satisfactorily describing the overall mechanism of decomposition necessitates considering all possible bimolecular reactions involving acetamide and 1-aminoethenol. For instance, the model for the unimolecular decomposition of acetamide does not account for the formation of acetic acid, that is, one of the three major experimental products. On the other hand, the overall experimentally determined activation energy for the formation of ammonia, acetonitrile and acetic acid from the self-condensation of acetamide is only 36.1 kcal/mol. Our results confirm the interpretation of Aspden et al[17] with regard to the importance of bimolecular-derived routes. Nevertheless, robust kinetic data for the unimolecular decomposition of acetamide is essential in the

pursuit of a better understanding of the self-decomposition of alkylated amides.

CONCLUSIONS

Optimized structures for intermediates, transition structures, and products are obtained for the salient reactions encountered in the pyrolysis of acetamide. The most energetically plausible exit pathways in the self-decomposition of acetamide are predicted to yield ammonia ($CH_3CONH_2 \rightarrow CH_2C(OH)NH_2 \rightarrow O{=}C{=}CH_2 + NH_3$) and acetonitrile ($CH_3CONH_2 \rightarrow CH_2C(OH)NH_2 \rightarrow N{\equiv}C{-}CH_3 + H_2O$) with overall activation barriers of 64.3 and 71.6 kcal/mol, respectively. However, the reverse reaction of acetamedic acid and 1-aminoethenol to form acetamide dominates their fragmentations into ammonia and acetonitrile, respectively. The direct decay of acetamide is found to be controlled by two competing channels: namely, $CONH_2 + CH_3$ and $O{=}C{=}CH_2 + NH_3$. In view of the results presented herein, it is anticipated that self-condensation of acetamide and other possible parallel bimolecular reactions play a major role in the pyrolysis of acetamide.

ASSOCIATED CONTENT

Supporting Information. Calculated total energies, zero-point energies, Cartesian coordinates, moments of inertia, and vibrational frequencies of all structures. This material is available free of charge via the Internet at http://pubs.acs.org.

AUTHOR INFORMATION

Corresponding Author

*Phone: +962 3 2179000. E-mail: mn.Alt@ahu.edu.jo

ACKNOWLEDGMENT

This study has been supported by a grant of computing time from the Australian Centre of Advanced Computing and Communications (ac3). R.A.P. is grateful to the Natural Sciences and Engineering Research Council of Canada (NSERC) for financial support. We also thank Professor John C. Mackie of the University of Newcastle, Australia, for a number of fruitful discussions.

REFERENCES

(1) Moldoveanu, S. C. Analytical Pyrolysis of Natural Organic Polymers; In *Techniques and Instrumentation in Analytical Chemistry*, Elsevier: Amsterdam, 1998.

(2) Fleischman, R. W.; Baker, J. R.; Hagopian, M.; Wade, G. G.; Hayden, D. W.; Smith, E. R.; Weisburger, J. H.; Weisburger, E. K. *J. Environ. Pathol. Toxicol.* **1980**, *3*, 149–170.

(3) Mirkova, E. T. *Mutat. Res.* **1996**, *352*, 23–30.

(4) Song, X.; Farwell, S. *J. Anal. Appl. Pyrolysis* **2004**, *71*, 901–915.

(5) Lal, G. S.; Hayes, E. R. *J. Anal. Appl. Pyrolysis* **1984**, *6*, 183–193.

(6) Fabbri, D.; Prati, S.; Vassura, I.; Chiavari, G. *J. Anal. Appl. Pyrolysis* **2003**, *68−69*, 163–171.

(7) Cao, J.; Zhao, X.; Morishita, K.; Wei, X.; Takarada, T. *Biores. Technol.* **2010**, *101*, 7648–7653.

(8) Yinon, J.; Yost, R.; Bulusub, S. *J. Chromatogr., A* **1994**, *688*, 231–242.

(9) Berwick, L.; Greenwood, P.; Kagi, R.; Croue, J. P. *Org. Geochem.* **2007**, *38*, 1073–1090.

(10) Stolarek, P.; Ledakowicz, S. *Thermochim. Acta* **2005**, *433*, 200–208.

(11) Sharma, R. K.; Chan, W. G. *J. Anal. Appl. Pyrolysis* **2004**, *72*, 153–163.

(12) Schmidt, H.; Tadjimukhamedov, F. K.; Douglas, K. M.; Prasad, S.; Smith, G. B.; Eiceman, G. A. *J. Anal. Appl. Pyrolysis* **2006**, *76*, 161–168.

(13) Yates, K.; Stevens, J. B. *Can. J. Chem.* **1965**, *43*, 529–537.

(14) Lee, I.; Kim, C. K.; Sed, H. S. *Tetrahedron* **1986**, *42*, 6627–6633.

(15) Hori, K.; Kamimura, A.; Ando, K.; Mizumura, M.; Ihara, Y. *Tetrahedron* **1997**, *53*, 4317–4333.

(16) Davidson, D.; Karten, M. *J. Am. Chem. Soc.* **1956**, *78*, 1066–1068.

(17) Aspden, J.; Maccoll, A.; Ross, R. A. *Trans. Faraday Soc.* **1967**, *64*, 965–976.

(18) Mackie, J. C.; Doolan, K. R. *Int. J. Chem. Kinet.* **1984**, *16*, 525541.

(19) Chen, X.-B.; Fang, W.-H.; Fang, D.-C. *J. Am. Chem. Soc.* **2003**, *125*, 9689–9698.

(20) Lee, D. S.; Gloyna, E. F. *Environ. Sci. Technol.* **1992**, *26*, 1587–1593.

(21) Frisch, M. J.; Trucks, G. W.; Schlegel, H. B.; Scuseria, G. E.; Robb, M. A.; Cheeseman, J. R.; Zakrzewski, V. G.; Montgomery, J. A.; Stratmann, R. E.; Burant, J. C.; et al. *Gaussian 03; revision A.11*; Gaussian, Inc.: Wallingford, CT, 2001.

(22) (a) Curtiss, L. A.; Raghavachari, K.; Redfern, P. C.; Rassolov, V.; Pople, A. *J. Chem. Phys.* **1998**, *109*, 7764–7772. (b) Baboul, A. G.; Curtiss, L. A.; Redfern, P. C.; Raghavachari, K. *J. Chem. Phys.* **1999**, *110*, 7650–7657.

(23) Curtiss, L. A.; Redfern, P. C.; Raghavachari, K.; Rassolov, V.; Pople, A. *J. Chem. Phys.* **1999**, *110*, 4703–4709.

(24) Montgomery, J. A.; Frisch, M. J., Jr.; Ochterski, J. W.; Petersson, G. A. *J. Chem. Phys.* **1999**, *110*, 2822–2827. (b) Montgomery, J. A., Jr.; Frisch, M. J.; Ochterski, J. W.; Petersson, G. A. *J. Chem. Phys.* **2000**, *112*, 6532–6542.

(25) Becke, A. D. *J. Chem. Phys.* **1996**, *104*, 1040–1046.

(26) Zhao, Y.; Lynch, B. J.; Truhlar, D. G. *J. Phys. Chem. A* **2004**, *108*, 2715–2719.

(27) Zhao, Y.; Gonzalez-Garcia, N.; Truhlar, D. G. *J. Phys. Chem. A* **2005**, *109*, 2012–2018.

(28) Montgomery, J. A.; n., Jr; Ochterski, J. W.; Petersson, G. A. *J. Chem. Phys.* **2000**, *112*, 6532–6542.

(29) Head-Gordon, M.; Pople, J. A.; Frisch, M. J. *Chem. Phys. Lett.* **1988**, *153*, 503–506.

(30) Eyring, H. *J. Chem. Phys.* **1935**, *33*, 107–115.

(31) McClurg, R. B.; Flagan, R. C.; Goddard, W. A. *J. Chem. Phys.* **1997**, *106*, 6675–6681.

(32) Mokrushin, V.; Bedanov, V.; Tsang, W.; Zachariah, M.; Knyazev, V. *ChemRate*; version 1.19; NIST: Gaithersburg, MD, 2002.

(33) Eckart, C. *Phys. Rev.* **1930**, *35*, 1303–1309.

(34) Fast, P. L; Truhlar, D. G. *J. Chem. Phys.* **1998**, *109*, 3721–3729.

(35) Pu, J.; Truhlar, D. G. *J. Chem. Phys.* **2002**, *117*, 1479–1481.

(36) Garrett, B. C.; Truhlar, D. G. *J. Chem. Phys.* **1979**, *70*, 1593–1598.

(37) Gilbert, R. G.; Smith, S. C. *Theory of Unimolecular and Recombination Reactions*; Blackwell Scientific: Oxford, 1990.

(38) Carstensen, H.-H.; Dean, A. M. The Kinetics of Pressure-Dependent Reactions. In *Comprehensive Chemical Kinetics*; Green, N., Ed.; Elsevier: London, 2007, Vol. 42, p 262.

(39) Hippler, H.; Troe, J.; Wendelken, H. J. *J. Chem. Phys.* **1982**, *78*, 6709–6717.

(40) Wong, M. W.; Wiberg, K. B. *J. Phys. Chem.* **1992**, *96*, 661–668.

(41) Prasad, B. V.; Grover, G.; Uppal, P.; Kaur, D. *J. Mol. Struct: THEOCHEM* **1999**, *458*, 227–237.

(42) Samdal, S. *J. Mol. Struct.: THEOCHEM* **1998**, *440*, 165–174.

(43) Kitano, M.; Kuchitsu, K. *Bull. Chem. Soc. Jpn.* **1973**, *46*, 3048–3051.

(44) Koijima, T.; Yano, E.; Nakagawa, K.; Tsunekawa, S. *J. Mol. Spectrosc.* **1987**, *122*, 408–416.

(45) Shi, J.; Huang, X.-Y.; Wang, J.-P.; Li, R. *J. Phys. Chem. A* **2010**, *114*, 6263–6272.
(46) Duan, X.; Page, M. *J. Am. Chem. Soc.* **1995**, *117*, 5114–5119.
(47) NIST Chemical Kinetics Database on the Web, *NIST Standard Reference Database 17, version 7.0*; available from http://kinetics.nist.gov/index.php.
(48) Yasunaga, K.; Kubo, S.; Hoshikawa, H.; Kamesawa, T.; Hidaka, Y. *Int. J. Chem. Kinet.* **2008**, *40*, 73–102.